Nodeless electron pairing in CsV3Sb5-derived kagome superconductors

Kozo Okazaki (okazaki@issp.u-tokyo.ac.jp)
Institute for Solid State Physics, University of Tokyo https://orcid.org/0000-0002-2334-918X
Yigui Zhong
University of Tokyo
Jinjin Liu
Beijing Institute of Technology
Xianxin Wu
Institute of Theoretical Physics, Chinese Academy of Sciences
Mine Akifumi
Institute for Solid State Physics, University of Tokyo
Yongkai Li
Beijing Institute of Technology, Chinese Academy of Sciences
Sahand Najafzadeh
Institute for Solid State Physics, University of Tokyo
Xinloong Han
University of Hong Kong https://orcid.org/0000-0001-8433-1648
Takeshi Kondo
ISSP, University of Tokyo https://orcid.org/0000-0002-3912-5172
Jiangping Hu
Institute of Physics https://orcid.org/0000-0002-4837-7742
Shik Shin
University of Tokyo https://orcid.org/0000-0002-2505-9362
Jia-Xin Yin
Princeton University https://orcid.org/0000-0003-2661-4206
Zhiwei Wang
Beijing Institute of Technology https://orcid.org/0000-0003-0182-2471
Xun Shi
Beijing Institute of Technology https://orcid.org/0000-0001-8719-911X
Yugui Yao
Beijing Institute of Technology https://orcid.org/0000-0003-3544-3787

Physical Sciences - Article

Keywords:

Posted Date: July 28th, 2022

DOI: https://doi.org/10.21203/rs.3.rs-1876119/v1

Nodeless electron pairing in CsV_3Sb_5-derived kagome superconductors

The newly discovered kagome superconductors represent a promising platform for investigating the quantum interplay between band topology, electronic order, and lattice geometry[1-8]. Despite extensive research efforts on this system, the nature of the superconducting ground state remains elusive[9-15]. In particular, consensus on the electron pairing symmetry has not been achieved so far[16-18], in part owing to the lack of a momentum-resolved measurement of the superconducting gap structure. Here we report the direct observation of a nodeless, nearly isotropic and orbital-independent superconducting gap in the momentum space of two exemplary CsV_3Sb_5-derived kagome superconductors — $Cs(V_{0.93}Nb_{0.07})_3Sb_5$ and $Cs(V_{0.86}Ta_{0.14})_3Sb_5$, using ultrahigh resolution and low temperature angle-resolved photoemission spectroscopy (ARPES). Remarkably, we find that such a gap structure is robust to the appearance or absence of charge order in the normal state, tuned by isovalent Nb/Ta substitutions of V. Moreover, the scaling ratio of gap versus superconducting transition temperature is close to the Bardeen-Cooper-Schrieffer (BCS) value, indicating a pairing in the weak-coupling regime. Our direct observation of the superconducting gap structure points to a persistent *s*-wave pairing in such kagome superconductors.

Superconductivity often emerges in the vicinity of other ordered electronic states with a broken symmetry, such as antiferromagnetic order and charge density wave. Their interdependence has been widely studied in cuprate and iron-based superconductors[19,20], while persists as a key issue for understanding the high temperature superconductivity. In certain cases, the ordered state and superconductivity can even coexist[21,22], which may indicate an unconventional pairing and have a dramatic impact on the superconducting mechanism. Because of the unique lattice geometry and unusual electronic features in a kagome lattice[1-3,23], the recently discovered kagome superconductors stand out as a new platform for inspecting the superconductivity emerging from a complex landscape of electronic orders[4,5,24,25]. Of particular interest is the nonmagnetic family of AV_3Sb_5 (A = K, Rb, Cs)[4,6], in which a variety of intriguing phenomena have been uncovered, including a tantalizing time-reversal symmetry broken charge density wave (CDW) order[7,8,26,27], a pair density wave[9], electronic nematicity[8,28-30], double superconducting domes under pressure[31,32] and giant anomalous Hall effect[33,34]. All these phenomena point out exotic intertwined effects in kagome superconductors AV_3Sb_5.

To identify the pairing nature and illuminate the pairing mechanism of such kagome superconductors, a fundamental issue is to reveal the superconducting (SC) gap structure, which remains elusive owing to the great challenge in resolving such small energy scales, and the existence of several conflicting experimental results. Taking CsV_3Sb_5 as an example, certain V-shaped gap as well as residual Fermi level states measured by scanning tunnelling spectroscopy[9,10,27] and a finite residual thermal conductivity towards zero temperature[11] seem to support a nodal SC gap. In contrast, the observations of the Hebel-Slichter coherence peak in the spin-lattice relaxation rate from the $^{121/123}$Sb nuclear quadrupole resonance measurement[12], and the exponentially temperature-dependent magnetic penetration depth[13,14], are more consistent with an *s*-wave superconductivity. Furthermore, the recent muon spin relaxation measurements on RbV_3Sb_5 superconductor reported a transition from the nodal to nodeless superconductivity by suppressing the charge order with applying pressure[15]. On the theoretical side, both unconventional and conventional superconducting pairing were proposed[16-18]. Therefore, an unambiguous characterization of the SC gap structure and its connection with the CDW order becomes an urgent necessity. During the long-term research of superconductors, ARPES has been proved to be a powerful tool to directly measure the SC gap in the momentum space[35,36]. Nevertheless, the relatively low transition temperature (T_c) and correspondingly small gap size render a thorough ARPES measurement extremely challenging.

In this work, we utilize an ultrahigh resolution and low temperature laser-ARPES, together with a chemical substitution of V in CsV_3Sb_5 that raises T_c, to precisely measure the gap structure in the superconducting state. CsV_3Sb_5 crystallizes in a layered structure with V atoms forming a 2D kagome net, as shown in the inset of Fig. 1a. At low temperatures, the material exhibits a CDW transition at T_{CDW} ~ 93 K, and eventually becomes superconducting at T_c ~ 3 K. In order to finely tune the competition between superconductivity and CDW, we take two elements to substitute V in CsV_3Sb_5. As shown in Fig. 1, both substitutions show a similar trend in the phase diagram, but with distinctions — Nb substitution enhances T_c more efficiently, while Ta dopant concentration can be increased to fully suppress the CDW order. Considering the accessibility in terms of temperature and the possible influence of CDW, we select $Cs(V_{0.93}Nb_{0.07})_3Sb_5$ and $Cs(V_{0.86}Ta_{0.14})_3Sb_5$, from two typical regions in the phase diagram, for the SC gap measurement (denoted hereafter as Nb0.07 and Ta0.14, respectively).

The Nb0.07 sample exhibits a T_c of 4.4 K and a T_{CDW} of 58 K, while the Ta0.14 sample exhibits a higher T_c of 5.2 K, but no clear CDW transition. Strikingly, as we shall present below, the gap structures of both samples are isotropic, regardless of the disappearance of CDW, hinting at a robust *s*-wave pairing.

Mapping out the Fermi surface (FS) is critical to investigate the SC gap structure, especially for a multiband system. Due to the limited detectable momentum area of 5.8-eV laser source, Fig. 2a shows a joint FS of the Ta0.14 sample by combing three segments. Similar to the pristine CsV_3Sb_5 sample[5,37,38], Ta0.14 sample has a circular electron-like pocket (marked as α) and a hexagonal hole-like pocket (marked as β) at the Brillouin zone (BZ) centre Γ point, and a triangle pocket (marked as δ) at the BZ corner K point. The α FS is formed by Sb 5*p* orbitals, while the β and δ FSs are derived from V 3*d* orbitals[37] and are close in momentum. As shown in Figs. 2a and 3b, the β and δ FSs are well distinguished due to the high momentum resolution of the laser source. Moreover, the intensities of β and δ FSs are enhanced under different polarizations of light (supplementary Note 1), which further makes the determination of the Fermi momentum (k_F) reliable.

Before investigating the SC gap structure, we first present the spectral evidence of the superconductivity below T_c. Using the Ta0.14 sample as an example, the temperature dependent energy distributed curves (EDCs) at k_F of a cut indicated in Fig. 2a are shown in Fig. 2b. At $T = 2$ K far below T_c, the emergence of the particle-hole symmetric quasiparticle peaks around Fermi level (E_F) clearly indicates the opening of an SC gap. With temperature gradually elevating, the growing intensity at E_F and the approaching quasiparticle peaks suggest that the SC gap becomes smaller and eventually closes. Quantitatively, the SC gap amplitude can be extracted from the fitting procedure based on a BCS spectral function (supplementary Note 2). The inset of Fig. 2b summarizes the SC gap amplitudes $\Delta(T)$ at different temperatures, which is fitted well with the BCS-like temperature function. The fitted SC gap amplitude at zero temperature, Δ_0, is ~ 0.77 meV, and the estimated T_c of ~ 5.2 K is consistent with the bulk T_c determined by resistivity measurement (Fig. 1c). These results demonstrate the high quality of the samples and the high precision of our SC gap measurements.

We then study the momentum dependence of the SC gap in the Ta0.14 sample, in which the CDW order is fully suppressed (Fig. 1b). Considering the six-fold symmetry of the FSs, we select various k_F points to cover the complete FS sheets and thus to capture the symmetry of the SC gap, as shown in Fig. 2f. The EDCs at k_F of the α, β and δ FSs are presented in Figs.

2c–e, respectively. For each k_F point, we take spectra below and above T_c, to ensure an *in-situ* precise comparison. In the vicinity of E_F, the leading edge of the EDCs at 2 K all show a shift compared to that at 7 K. Moreover, they universally show a strong coherence peak at a binding energy E_B of ~ 1 meV, indicating a rather isotropic SC gap structure. Fitting these EDCs to a BCS spectral function, the quantitatively extracted SC gap amplitudes are summarized in Fig. 2g. These SC gaps of different FSs have rarely fluctuated amplitudes with an average Δ_{Ta} of 0.77 ± 0.06 meV, yielding the ratio $2\Delta_{Ta}/k_BT_c$ of 3.44 ± 0.27, which is remarkably close to the BCS value of ~3.53 for *s*-wave superconductivity. These results clearly demonstrate an isotropic SC gap and support a weak-coupling superconductivity in the Ta0.14 sample.

Next, we turn to examine the possible influence of the CDW order in the normal state on the superconducting pairing symmetry[15,31]. We measure the SC gap structure of the Nb0.07 sample, where T_{CDW} gets slightly suppressed, and T_c is smoothly elevated from that of the pristine CsV_3Sb_5 (Fig. 1a). In this sense, the superconductivity in the Nb0.07 sample is expected to have a similar SC gap structure with CsV_3Sb_5. As shown in Fig. 3a, the FS topology of the Nb0.07 sample is also similar to that of CsV_3Sb_5, consisting of the circular α FS, hexagonal β FS and triangular δ FS, which is consistent with the previous ARPES measurements[39] and the calculations based on density function theory[40] (supplementary Fig. S3). The EDCs at k_F positions indicated in Fig. 3f, on these three FSs, are presented in Figs. 3c–e, respectively. Just like the case of the Ta0.14 sample, coherence peaks raise up at a similar energy position for all EDCs at 2 K, albeit of a slightly broader shape due to a smaller SC gap and lower T_c. By fitting the EDCs to the BCS spectral function, the SC gap amplitudes along the FSs are summarized in Fig. 3g. The data clearly shows a nearly isotropic SC gap structure in the Nb0.07 sample, with the gap amplitude Δ_{Nb} of 0.54 ± 0.06 meV, giving a ratio $2\Delta_{Nb}/k_BT_c$ of 2.83 ± 0.32, which is smaller than the BCS value. Nevertheless, our results show that an isotropic SC gap robustly persists in the Nb0.07 sample, and the system is still in a weak-coupling regime, regardless of the CDW order.

As the kagome metals AV_3Sb_5 have a three-dimensional electronic structure[37,38], we further examine the SC gap at another k_z plane through tuning the photon energy from 5.8 eV to 7 eV. We find that the SC gap remains nearly the same at these two k_z planes within our experimental uncertainties (supplementary Fig. S4). Giving the direct momentum-resolving capability of ARPES, and the prominent features of SC gap opening throughout the whole BZ, our data unambiguously reveal a nodeless, nearly isotropic and orbital-independent SC gap in both Nb0.07 and Ta0.14 samples (Figs. 4a, b).

These results shine a light on the interplay between superconductivity and unconventional CDW in CsV_3Sb_5. As shown in Fig. 4c and Fig. S5, the isovalent substitutions of Nb/Ta for V in our experiments do not change the crystal structure and can be viewed as an effective in-plane negative pressure, which suppresses the CDW order while enhances the superconductivity. When the superconductivity emerges from the CDW order, our measurements on the Nb0.07 sample reveal a nearly isotropic gap structure (Fig. 4a). Once the CDW order is eliminated through a larger lattice expansion induced by 14%-Ta substitution of V, the superconducting gap amplitude gets enhanced, but the gap structure remains nodeless and isotropic (Fig. 4b). Our results uncover a robust full SC gap across the CDW suppression (Fig. 4c), different to the muon spin relaxation measurements which reported a transition from nodal to nodeless pairing in pressurized RbV_3Sb_5[15]. The difference between two regimes, represented by Nb0.07 and Ta0.14 samples, is that the ratio $2\Delta/k_BT_c$ being smaller than the BCS value when superconductivity coexists with the CDW order. This may be attributed to the CDW order partially gapping out the FSs and generating spin polarizations before entering the superconducting phase. Our results suggest that the CDW actively competes with the superconductivity in a way of dissipating superfluid density rather than dramatically altering pairing symmetry in CsV_3Sb_5 family materials. It is worth mentioning that the anomalous Hall effect, which is commonly observed in AV_3Sb_5 and possibly related to the time-reversal symmetry breaking[7,33,34], is found to be weakened in Nb0.07 while disappeared in Ta0.14, as shown in supplementary Fig. S6. This suggests that the anomalous Hall effect is intimately correlated to the CDW[34,40], showing little impact on the superconducting pairing.

Finally, our results directly come to the point of the pairing symmetry and superconductivity mechanism in CsV_3Sb_5 family. Correlation effect[3,26] and van Hove singularities[23,37,38] associated with the V 3*d* orbitals in the kagome lattice are considered to play a pivotal role in the intriguing phenomena in AV_3Sb_5 superconductors[6]. They could give rise to a nodal or a nodeless pairing but with strong anisotropy[16,17]. From this point of view, the SC gap is expected to exhibit noticeable orbital dependence due to the distinct electronic correlations, which is, however, inconsistent with our results. A natural and straightforward scenario inspired by the isotropic SC gap with the ratio $2\Delta/k_BT_c$ close to the BCS value is the orbital independent *s*-wave pairing. This is further supported by our observations of the electron-phonon coupling induced band dispersion kinks in both the pristine CsV_3Sb_5[41,42] and substituted samples, as well as the positive relation between the coupling strength and the superconducting transition temperature (supplementary Fig. S7). In this scenario, the isotropic

SC gap is expected to be robust against tuneable CDW, anomalous Hall effect and lattice expansion, as summarized in Table 1. Thereby, our unambiguous observations of the isotropic SC gap, in two exemplary samples with distinct properties, suggest that the *s*-wave pairing symmetry is mostly favoured for the CsV_3Sb_5 family, anchoring the direction for the superconductivity mechanism of the AV_3Sb_5 kagome superconductors.

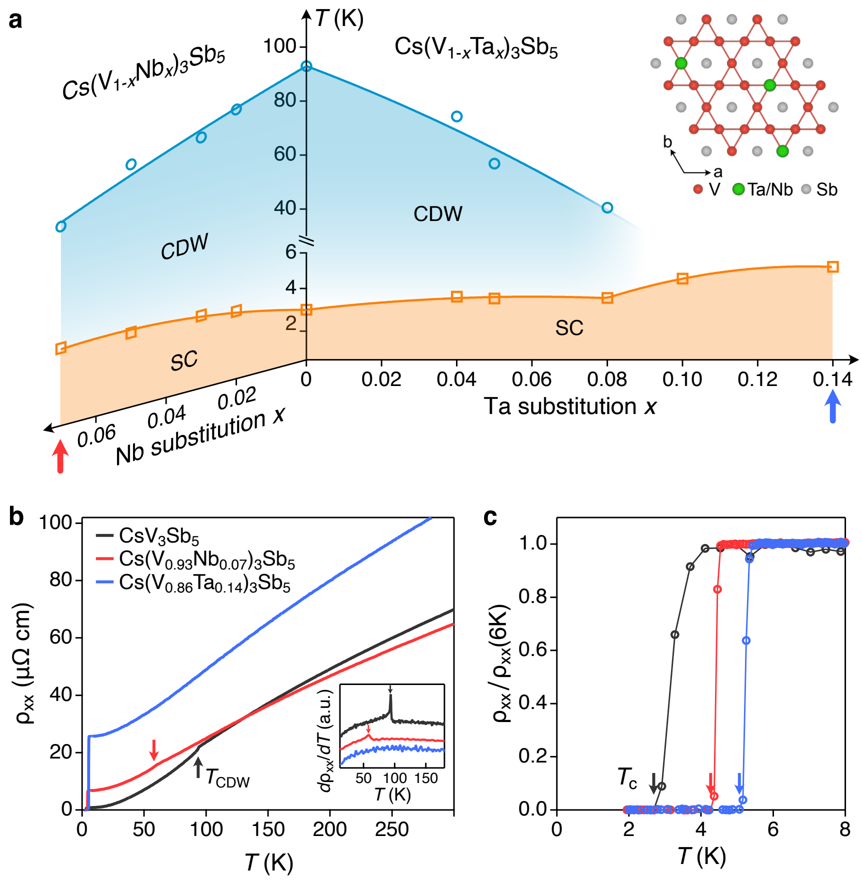

Fig. 1. Evolution of CDW and superconductivity in CsV_3Sb_5 upon chemical substitutions. a, Phase diagrams for $Cs(V_{1-x}Nb_x)_3Sb_5$ and $Cs(V_{1-x}Ta_x)_3Sb_5$. Inset: the lattice structure of V-Sb layer, illustrating the Ta or Nb substitution of V atoms within the kagome lattice. **b**, Temperature dependence of in-plane resistivity for the pristine and two substituted samples studied in this work. The arrows indicate the anomalies associated with CDW transitions. The inset shows the differential resistivity to highlight the CDW transitions, with the curves vertically shifted for clarity. Note that there is no CDW order observed in $Cs(V_{0.86}Ta_{0.14})_3Sb_5$. **c**, Normalized resistivity curves in the low temperature range showing clear superconducting transitions.

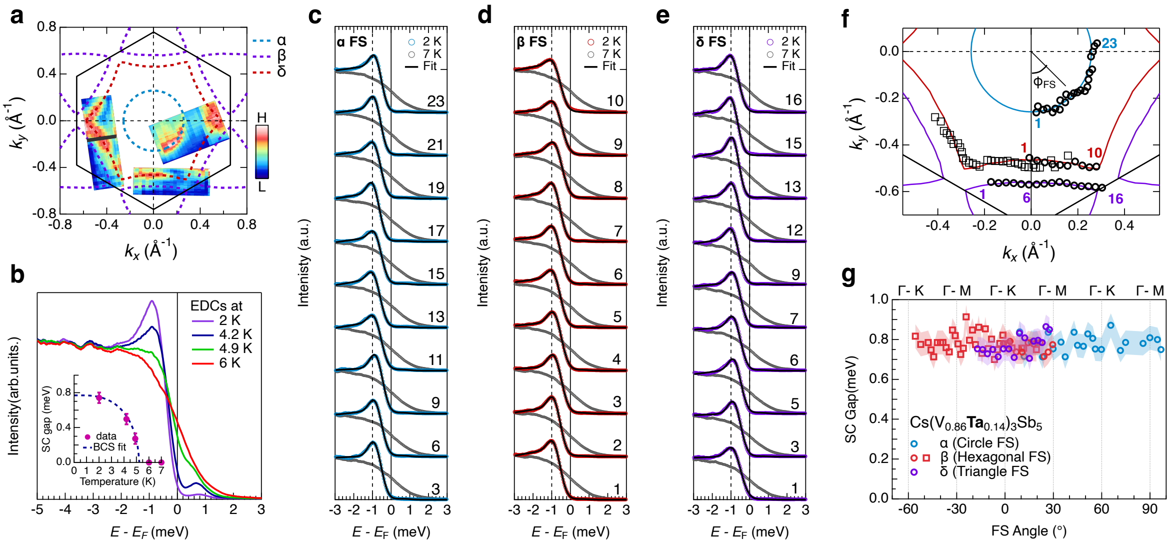

Fig. 2. Isotropic superconducting gap in $Cs(V_{0.86}Ta_{0.14})_3Sb_5$. a, ARPES intensity integrated over ± 5 meV around E_F. The broken lines represent the FS contours. **b**, Temperature dependence of EDC at k_F in a cut marked as black line in **a**. Inset shows the temperature dependent SC gap amplitude determined by the fitting procedure based on the BCS spectral function. The blue broken curve represents BCS-like temperature dependence. **c-e**, EDCs at k_F measured at T = 2 K and 7 K along with the α, β and δ FSs, respectively. The k_F positions of these EDCs are summarized in **f** as black thick circles. The black lines are the curves fitted by BCS spectral function. The dashed lines mark the peak of the EDCs. **g**, SC gap magnitude estimated from the fits to EDCs shown in **c-e**. The shaded areas represent the error bars determined from the standard deviation of E_F. The square makers are the SC gap results from an independent sample and the corresponding k_F are shown as thin square in **f**.

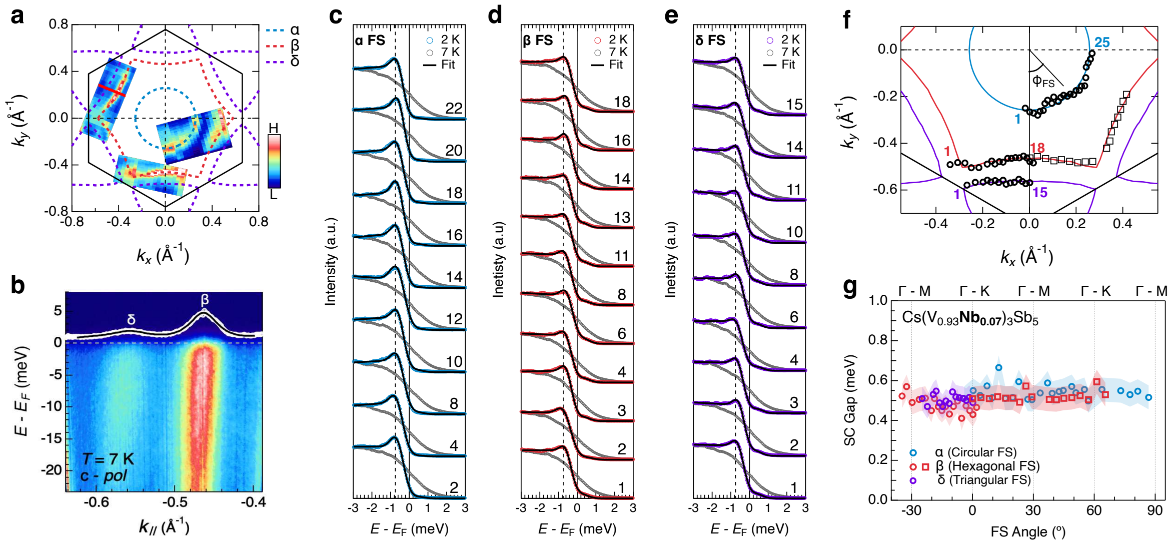

Fig. 3. Isotropic superconducting gap in charge ordered $Cs(V_{0.93}Nb_{0.07})_3Sb_5$. a, ARPES intensity integrated over ± 5 meV around E_F. The broken lines represent the calculated FS contours. **b**, ARPES intensity plot along a red line shown in **a**. The intensity is measured using circular polarization to capture both β and δ bands. The white dotted line represents the MDC integrated over ± 2 meV around E_F and the black line is a double-peak Lorentzian fit. Two distinguished peaks in the MDC shows k_F positions of the β and δ bands. **c-e**, EDCs at k_F taken along the α, β and δ FSs, respectively. The k_F positions of these EDCs are summarized in **f**. The dashed lines mark the estimated peak position of the EDCs. The black lines are the curves fitted by BCS spectral function. **g**, SC gap magnitude estimated from the fits to EDCs shown in **c-e**. The square makers are the SC gap results from an independent sample and the corresponding k_F are shown as thin square in **f**. The shaded areas represent the error bars determined from the standard deviation of E_F.

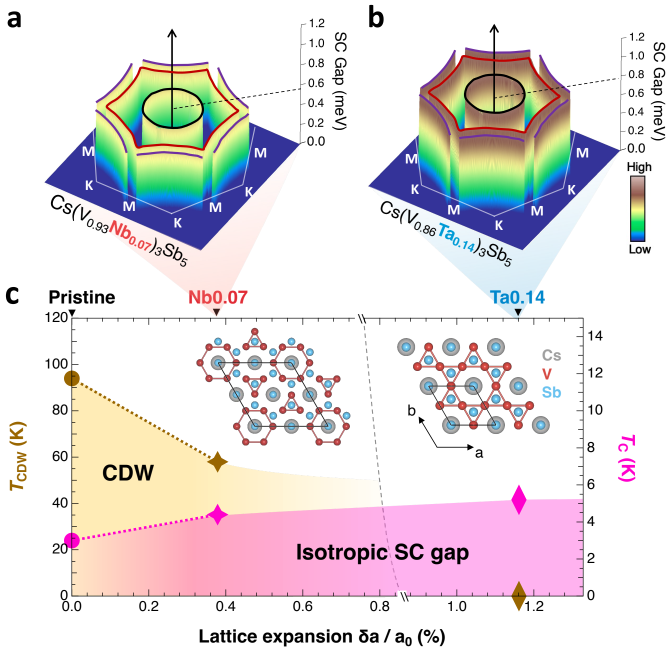

Fig. 4. Robust isotropic SC gap upon suppression of CDW. a-b, Schematic momentum dependence of the SC gap magnitude of the Nb0.07 and Ta0.14 samples, respectively. **c,** Schematic phase diagram in which T_{CDW} and T_c are plotted as function of the lattice expansion due to the chemical substitutions. The lattice expansion is represented by $\delta a/a_0$, where $\delta a = a - a_0$ is the change of the in-plane lattice constant a from that of pristine CsV_3Sb_5 (a_0). The inset shows the lattice structures of the CDW (left) and undistorted (right) phases, representing the states above T_c for two distinct regions in the phase diagram. The black solid lines in the insets mark the corresponding single-unit cells. The isotropic SC gap symmetry persists through such two regions, regardless of the existence of a CDW order.

Sample / Properties	CsV_3Sb_5	$Cs(V_{0.93}Nb_{0.07})_3Sb_5$	$Cs(V_{0.86}Ta_{0.14})_3Sb_5$
***Lattice constant a* (Å)**	**5.4949**	**5.5157**	**5.5587**
Superconductivity	**3 K**	**4.4 K**	**5.2 K**
Charge density wave	**93 K**	**65 K**	✗
Anomalous Hall effect	✓	✓	✗
EPC induced band kink	✓	✓	✓
Pairing gap symmetry	**-**	**isotropic**	**isotropic**

Table 1. Summary of the physical properties of pristine CsV_3Sb_5, $Cs(V_{0.93}Nb_{0.07})_3Sb_5$ and $Cs(V_{0.86}Ta_{0.14})_3Sb_5$ samples. The details about anomalous Hall effect and electron-phonon coupling (EPC) induced kink are demonstrated in Figs. S6 and S7, respectively.

Methods

Growth of single crystals. High-quality single crystals of $Cs(V_{0.86}Ta_{0.14})_3Sb_5$ and $Cs(V_{0.93}Nb_{0.07})_3Sb_5$ were synthesized from Cs bulk (Alfa Aesar, 99.8%), V piece (Aladdin, 99.97%), Ta powder (Alfa Aesar, 99.99%), and Sb shot (Alfa Aesar, 99.9999%), via a self-flux method using $Cs_{0.4}Sb_{0.6}$ as flux. The above starting materials were put into an aluminium crucible and sealed in a quartz tube, which was then heated to 1000°C in 24h and dwelt for 200 h. After that, the tube was cooled to 200°C at a rate of 3°C/h, followed by cooling down to room temperature with the furnace switched off. In order to remove the flux, the obtained samples were soaked in deionized water. Finally, shiny single crystals with hexagonal feature were obtained.

Electronic transport measurements. Electronic transport properties of $Cs(V_{0.86}Ta_{0.14})_3Sb_5$ and $Cs(V_{0.93}Nb_{0.07})_3Sb_5$ crystals were measured on a physical property measurement system (PPMS, Quantum Design) at a temperature range from 300 K to 1.8 K. Five-terminal method was used, at which the longitudinal resistivity and Hall resistivity can be taken simultaneously. DC magnetic susceptibility was measured on a magnetic property measurement system (MPMS, Quantum Design) with a superconducting quantum interference device (SQUID) magnetometer.

High-resolution laser-ARPES measurements. Ultrahigh-resolution ARPES measurements were performed in a laser-based ARPES setup, which consisted of a continuous wave laser (hυ = 5.8 eV) and a vacuum ultraviolet laser (hυ = 6.994 eV), a Scienta HR8000 hemispherical analyser, and a sample manipulator cooled by decompression-evaporative the liquid helium. The samples were *in-situ* cleaved and measured under a vacuum better than 3×10^{-11} torr. The sample temperature was varied from 2 to 7 K, and the energy resolution for the superconducting gap measurements was better than 0.6 meV for 5.8-eV laser and 1.5 meV for 6.994-eV laser. The Fermi level E_F was calibrated with an *in-situ* connected gold reference.

Competing interests: The authors declare no competing interests.

Data availability: Data are available from the corresponding author upon reasonable request.

References:

1 Syôzi, I. Statistics of kagomé lattice. *Progress of Theoretical Physics* **6**, 306-308 (1951).
2 Guo, H.-M. & Franz, M. Topological insulator on the kagome lattice. *Physical Review B* **80**, 113102 (2009).

3 Kiesel, M. L. & Thomale, R. Sublattice interference in the kagome Hubbard model. *Physical Review B* **86**, 121105 (2012).
4 Ortiz, B. R. *et al.* New kagome prototype materials: discovery of KV_3Sb_5, RbV_3Sb_5, and CsV_3Sb_5. *Physical Review Materials* **3**, 094407 (2019).
5 Ortiz, B. R. *et al.* CsV_3Sb_5: A Z_2 Topological Kagome Metal with a Superconducting Ground State. *Physical Review Letters* **125**, 247002 (2020).
6 Neupert, T., Denner, M. M., Yin, J.-X., Thomale, R. & Hasan, M. Z. Charge order and superconductivity in kagome materials. *Nature Physics* **18**, 137-143 (2021).
7 Mielke, C. *et al.* Time-reversal symmetry-breaking charge order in a kagome superconductor. *Nature* **602**, 245-250 (2022).
8 Jiang, Y.-X. *et al.* Unconventional chiral charge order in kagome superconductor KV_3Sb_5. *Nature Materials* **20**, 1353-1357 (2021).
9 Chen, H. *et al.* Roton pair density wave in a strong-coupling kagome superconductor. *Nature* **599**, 222-228 (2021).
10 Xu, H.-S. *et al.* Multiband superconductivity with sign-preserving order parameter in kagome superconductor CsV_3Sb_5. *Physical Review Letters* **127**, 187004 (2021).
11 Zhao, C. *et al.* Nodal superconductivity and superconducting domes in the topological Kagome metal CsV_3Sb_5. *arXiv:2102.08356* (2021).
12 Mu, C. *et al.* S-wave superconductivity in kagome metal CsV_3Sb_5 revealed by $^{121/123}Sb$ NQR and ^{51}V NMR measurements. *Chinese Physics Letters* **38**, 077402 (2021).
13 Duan, W. *et al.* Nodeless superconductivity in the kagome metal CsV_3Sb_5. *Science China Physics, Mechanics & Astronomy* **64**, 107462 (2021).
14 Gupta, R. *et al.* Microscopic evidence for anisotropic multigap superconductivity in the CsV_3Sb_5 kagome superconductor. *npj Quantum Materials* **7**, 49 (2022).
15 Guguchia, Z. M. I., C *et al.* Tunable nodal kagome superconductivity in charge ordered RbV_3Sb_5. *arXiv:2202.07713* (2022).
16 Wu, X. *et al.* Nature of Unconventional Pairing in the Kagome Superconductors AV_3Sb_5 (A=K, Rb, Cs). *Physical Review Letters* **127**, 177001 (2021).
17 Tazai, R., Yamakawa, Y., Onari, S. & Kontani, H. Mechanism of exotic density-wave and beyond-Migdal unconventional superconductivity in kagome metal AV_3Sb_5 (A= K, Rb, Cs). *Science Advances* **8**, eabl4108 (2022).
18 Gu, Y., Zhang, Y., Feng, X., Jiang, K. & Hu, J. Gapless excitations inside the fully gapped kagome superconductors AV_3Sb_5. *Physical Review B* **105**, L100502 (2022).
19 Keimer, B., Kivelson, S. A., Norman, M. R., Uchida, S. & Zaanen, J. From quantum matter to high-temperature superconductivity in copper oxides. *Nature* **518**, 179-186 (2015).
20 Fernandes, R. M. *et al.* Iron pnictides and chalcogenides: a new paradigm for superconductivity. *Nature* **601**, 35-44 (2022).
21 Ge, Q. *et al.* Anisotropic but nodeless superconducting gap in the presence of spin-density wave in iron-pnictide superconductor $NaFe_{1-x}Co_xAs$. *Physical Review X* **3**, 011020 (2013).
22 He, R.-H. *et al.* Energy gaps in the failed high-T_c superconductor $La_{1.875}Ba_{0.125}CuO_4$. *Nature Physics* **5**, 119-123 (2009).
23 Wang, W.-S., Li, Z.-Z., Xiang, Y.-Y. & Wang, Q.-H. Competing electronic orders on kagome lattices at van Hove filling. *Physical Review B* **87**, 115135 (2013).
24 Mielke III, C. *et al.* Nodeless kagome superconductivity in $LaRu_3Si_2$. *Physical Review Materials* **5**, 034803 (2021).
25 Mielke III, C. *et al.* Local spectroscopic evidence for a nodeless magnetic kagome superconductor $CeRu_2$. *arXiv:2204.00341* (2022).
26 Zhao, H. *et al.* Cascade of correlated electron states in the kagome superconductor CsV_3Sb_5. *Nature* **599**, 216-221 (2021).

27 Wang, Z. *et al.* Electronic nature of chiral charge order in the kagome superconductor CsV_3Sb_5. *Physical Review B* **104**, 075148 (2021).
28 Xiang, Y. *et al.* Twofold symmetry of c-axis resistivity in topological kagome superconductor CsV_3Sb_5 with in-plane rotating magnetic field. *Nature communications* **12**, 6727 (2021).
29 Li, H. *et al.* Rotation symmetry breaking in the normal state of a kagome superconductor KV_3Sb_5. *Nature Physics* **18**, 265–270 (2022).
30 Miao, H. *et al.* Geometry of the charge density wave in the kagome metal AV_3Sb_5. *Physical Review B* **104**, 195132 (2021).
31 Chen, K. *et al.* Double superconducting dome and triple enhancement of T_c in the kagome superconductor CsV_3Sb_5 under high pressure. *Physical Review Letters* **126**, 247001 (2021).
32 Yu, F. *et al.* Unusual competition of superconductivity and charge-density-wave state in a compressed topological kagome metal. *Nature communications* **12**, 3645 (2021).
33 Yang, S.-Y. *et al.* Giant, unconventional anomalous Hall effect in the metallic frustrated magnet candidate, KV_3Sb_5. *Science advances* **6**, eabb6003 (2020).
34 Yu, F. *et al.* Concurrence of anomalous Hall effect and charge density wave in a superconducting topological kagome metal. *Physical Review B* **104**, L041103 (2021).
35 Richard, P., Qian, T. & Ding, H. ARPES measurements of the superconducting gap of Fe-based superconductors and their implications to the pairing mechanism. *Journal of Physics: Condensed Matter* **27**, 293203 (2015).
36 Sobota, J. A., He, Y. & Shen, Z.-X. Angle-resolved photoemission studies of quantum materials. *Reviews of Modern Physics* **93**, 025006 (2021).
37 Hu, Y. *et al.* Rich nature of Van Hove singularities in Kagome superconductor CsV_3Sb_5. *Nature Communications* **13**, 2220 (2022).
38 Kang, M. *et al.* Twofold van Hove singularity and origin of charge order in topological kagome superconductor CsV_3Sb_5. *Nature Physics* **18**, 301–308 (2022).
39 Kato, T. *et al.* Fermiology and Origin of T_c Enhancement in a Kagome Superconductor Cs $(V_{1-x}Nb_x)_3Sb_5$. *arXiv:2205.04907* (2022).
40 Li, Y. *et al.* Tuning the competition between superconductivity and charge order in the kagome superconductor $Cs(V_{1-x}Nb_x)_3Sb_5$. *Physical Review B* **105**, L180507 (2022).
41 Luo, H. *et al.* Electronic nature of charge density wave and electron-phonon coupling in kagome superconductor KV_3Sb_5. *Nature Communications* **13**, 1-8 (2022).
42 Zhong, Y. *et al.* Testing electron-phonon coupling for the superconductivity in Kagome metal CsV_3Sb_5. *arXiv:2207.02407* (2022).

Supplementary Files

This is a list of supplementary files associated with this preprint. Click to download.

- SICVSSCgap.pdf